

The Formation of Population III Binaries from Cosmological Initial Conditions

Matthew J. Turk,^{1*} Tom Abel,¹ Brian O’Shea²

¹Kavli Institute for Particle Astrophysics and Cosmology, Stanford University,
2575 Sand Hill Road, Menlo Park, CA 94025,

²Department of Physics & Astronomy, Michigan State University, East Lansing, MI 48824-2320

*To whom correspondence should be addressed; E-mail: mturk@slac.stanford.edu.

Previous high resolution cosmological simulations predict the first stars to appear in the early universe to be very massive and to form in isolation. Here we discuss a cosmological simulation in which the central $50M_{\odot}$ clump breaks up into two cores, having a mass ratio of two to one, with one fragment collapsing to densities of 10^{-8}g cm^{-3} . The second fragment, at a distance of ~ 800 astronomical units, is also optically thick to its own cooling radiation from molecular hydrogen lines, but is still able to cool via collision-induced emission. The two dense peaks will continue to accrete from the surrounding cold gas reservoir over a period of $\sim 10^5$ years and will likely form a binary star system.

Hydrodynamical simulations that start from cosmological initial conditions have predicted that the first luminous objects in the universe were isolated stars with masses in the range $30 - 300M_{\odot}$, based on accretion rates calculated in the absence of accretion-inhibiting factors (1–3). Idealized protostellar evolution simulations suggest accretion should end when the star reaches $\sim 100M_{\odot}$ (4), but even though most relevant feedback mechanisms of the protostars on their accretion flow are known (5), no fully self-consistent radiation hydrodynamical simulations reaching the main sequence have yet been possible, even in one dimension. The early stages of proto-stellar evolution, however, are understood in some detail from spherically symmetric calculations (6, 7) as well as semi-analytic models (8).

The environment in which the first stars form is calculated by following early-universe evolution of the primordial gas and dark matter; by this means, the first stars are found to

form in halos with a total mass of $\sim 10^6 M_\odot$, with collapse driven first by cooling via molecular hydrogen ro-vibrational lines and later by collision induced emission (6, 9, 10). While several tens of calculations (1, 11, 12) have followed the collapse of a primordial protostellar halo to relatively low densities ($\sim 10^{-12} \text{g cm}^{-3}$), only two previous calculations have followed the collapse from cosmological initial conditions to protostellar densities (2, 13). Both of these calculations utilized a chemical model that included the relevant medium- and high-density physics, such as heating from the formation of molecular hydrogen, collisionally induced emission, three-body molecular hydrogen formation, and gas opacity at high densities. Several simulations have followed the collapse of a single metal-free cloud starting from idealized initial conditions (3, 14, 15). Parameter studies of rotating cylinders have shown that metal-free gas can fragment (16) and have found fragmentation of spherical distributions of extremely low- and zero-metallicity gas (17), including in 3D nested grid parameter studies (18). Additionally, studies of zero-metallicity gas collapsing in isolation have found fragmentation at low densities ($\sim 10^{-16} \text{g cm}^{-3}$) (19). However, no previous simulation starting from cosmological initial conditions has shown fragmentation in a cosmological context.

We present simulations performed with the adaptive mesh refinement code Enzo (O’Shea *et al.*(2004)). These simulations were initialized at a redshift of 99 in a box 300kpc h^{-1} (comoving). (Detailed simulation parameters and methods can be found in the supporting online material.) We stopped the simulation at a maximum (proper) baryon density of $1.61 \times 10^{-8} \text{g cm}^{-3}$ at $z = 19.08$ (189 million years after the Big Bang) and $1.72 R_\odot$ (proper) peak spatial resolution, where we have resolved the first massive halo that forms in this simulation volume. The simulation presented here is explicitly a simulation of the first generation of Population III star formation. The second generation of Population III stars are still primordial in composition but are affected by previous generation of stars, potentially by effects such as kinetic energy injection, radiation backgrounds or cosmic rays. We have simulated five realizations of first-generation Population III stars that evolve to at least this density and have found fragmentation in one. The dark matter halo merger history and the evolution of baryonic properties at redshifts above 20 are typical of previous simulations (1, 20).

The collapsing halo fragmented at a density of $\simeq 2.0 \times 10^{-13} \text{g cm}^{-3}$ at redshift $z = 19.08$, roughly. We have conducted resolution studies, where we found fragmentation but a change in the separation of the identified cores. (More information can be found in the supporting online materials.) To study the fragmentation of the cloud, we identified gravitationally-bound, topologically-connected regions at or above a single density within the halo’s virial radius. The density at which these regions diverged was $\sim 2.0 \times 10^{-13} \text{g cm}^{-3}$, however, because the difference was only a thin strip of lower density gas, we conducted all subsequent analysis on connected isodensity surfaces with minimum density of $3.0 \times 10^{-13} \text{g cm}^{-3}$. We selected material within two isodensity surfaces, hereafter referred to as Core A and Core B (*Fig. 1*). Core A is the more massive core, with a mass of $10.0 M_\odot$, and Core B of $6.3 M_\odot$. Determining whether these two objects will

ultimately merge is nontrivial, but estimates can be made based on the current orbital mechanics as well as collapse conditions of each core in isolation. If these two objects form hydrostatically-supported protostellar cores and most of the intervening gas is accreted onto them, they will remain separate and form a binary star system.

Both cores are oblate and are embedded in a crescent-shaped cloud. Even though they can not be reliably identified more than ~ 175 years before the end of the simulation, the beginning of fragmentation is already evident in both density and molecular hydrogen, where lower-density, mostly-atomic regions are permeated by filaments of higher-molecular fraction gas. (*Fig. 1*, top row.) Averaging over the time period during which the two cores are identifiable and distinct, Core A experiences $0.061 M_{\odot}/\text{year}$ mass flux across its density isosurface, while Core B has mass flux of $0.049 M_{\odot}/\text{year}$. (*Fig. 2*) The flow across both density isosurfaces is roughly linear. The peak densities in both cores evolve at close to free-fall trajectories and Core B collapses ~ 60 years after Core A.

The separation of the centers of mass of the two cores is 800AU. Within a minimally enclosing sphere of radius 780AU located at the center of mass of the two cores, we find a total mass of $52M_{\odot}$; within a sphere of radius twice the separation of the cores, we find a mass of $99 M_{\odot}$. By defining

$$\bar{R} = \left(\frac{3M_{\text{enc}}}{4\pi\bar{\rho}} \right)^{1/3}$$

we calculated the characteristic radius of each core. Core B, the lower-mass core, is at this time less dense than Core A, and has a smaller characteristic radius. Given its current angular momentum and assuming both angular momentum conservation and no material between the cores its final Keplerian radius is given by

$$R_{\text{kep}} = \frac{L_B^2}{GM_A}$$

where L_B is the specific angular momentum of Core B in the rest frame of Core A and M_A is the mass of Core A. R_{kep} evaluates to 2400 AU, which is three times their current distance, indicating that the velocity of Core B is super-Keplerian. The tangential velocity of Core B with respect to Core A is 5.9 km s^{-1} , and it has a radial velocity of -5.3 km s^{-1} . Given the current velocities, separation and masses of the cores and the assumption that the two cores exist with their current trajectories in a vacuum, a simple orbit integration shows that their closest approach of 480 AU would occur after 360 years, more than 10 dynamical times of the lighter core. However, this vacuum assumption could be misleading. Another limit can be derived assuming the remaining $46M_{\odot}$ mass between Core A and B instantaneously were accreted onto only Core A, then the orbit integrations show it would take over 400 years for B to come within 300 AU of A. Because the time scale of the formation of hydrostatically-supported, protostellar cores in either core is close to the free fall time, an accreting binary system will form. Following the formulation of the dynamical friction force on a massive perturber in a near-circular orbit (21), the

loss of angular momentum through dynamical friction does not substantially increase the likelihood of a merger of the two cores; in fact, by providing an upper bound on the infall rate, we see that both cores will form protostars long before merging. We have calculated the average density of the background medium using spheres both two and five times the radius of the core separation and found that the two cores should not approach closer than 100 AU for at least 3600 years.

We plotted radially-binned, mass-weighted average quantities at several epochs of the halo collapse. (Fig. 3) The central bin was located at the most dense zone in the simulation at all times. After the cloud fragmented, this most dense zone was always within Core A. The location of Core B is clearly visible as a spike in the density, temperature, and H₂ fraction, and a slight enhancement in the enclosed mass, at ~ 800 AU. The temperature plot shows a marked increase at high densities compared to that of both previous studies (1, 11). This is likely a result not only of different molecular hydrogen formation and cooling rates, and also the inclusion of the heating from the formation of molecular hydrogen and opacity to molecular hydrogen lines. These factors delay the conversion to a fully-molecular state until the gas collapses to higher densities, reducing the efficiency of the ro-vibrational cooling, leading to higher temperatures. Furthermore, the average molecular hydrogen fraction of the cloud does not reach unity, as it has in previous calculations. At higher densities the cooling from ro-vibrational lines is inefficient as a result of increased optical depth; this leads to an increase in the temperature, and thus a drop in the molecular hydrogen fraction. There is no substantial dissociation at the final output of this simulation, but the inner region of the collapsing halo has a molecular hydrogen mass fraction of ~ 0.5 . As the cloud collapses further, H₂ will dissociate at densities just slightly higher than those presented here. Following the prescription of (9), the peak density of the simulation provides an effective transmission coefficient of 2×10^{-3} for ro-vibrational cooling and a transmission coefficient of 0.94 for cooling from collision induced emission.

To estimate instabilities brought on by chemical and radiative mechanisms, we follow the methods of (9); when the characteristic timescales for the change in energy of the gas is less than the dynamical time, small perturbations can no longer be effectively suppressed and the gas is susceptible to fragmentation. The dynamical time is defined by

$$t_{\text{dyn}} \equiv \sqrt{\frac{3\pi}{16G\rho}}$$

By defining E as the total thermal energy of the gas, \dot{e}_{rad} as the radiative cooling from ro-vibrational lines and collision-induced emission, and \dot{e}_{chem} as the heating or cooling due to chemical changes in the molecular hydrogen content of the gas (4.48 eV per molecule), we can write the molecular hydrogen timescale as

$$t_{\text{H}_2} = \frac{E}{\dot{e}_{\text{rad}} - \dot{e}_{\text{chem}}}$$

Comparing these two quantities (Fig. 4) we found that the ratio was approximately unity at most densities, but that at the densities at which the gas fragmented, this ratio changed sign abruptly. This is a steep transition, from being moderately prone to fragmentation, to being dominated by the heating from the formation of H₂. However, as shown by (22), in isolation the thermal instability brought on by the onset of three-body heating and molecular line cooling would not be sufficient to cause the fragmentation of a collapsing gas cloud.

We define the rotational energy as

$$E_{\text{rot}} \equiv \frac{1}{2} \omega \mathbf{I} \omega$$

where ω is the rotational velocity and \mathbf{I} is the inertial tensor of the gas. For a sphere of radius r and mass M the gravitational binding energy W is

$$W \equiv \frac{3}{5} \frac{GM^2}{r}$$

We compared these two quantities (Fig. 4, bottom) and indicated with thin lines the critical ratios of ~ 0.44 (23) and 0.27 (24) above which dynamical instabilities can become dominant in compressible toroids and compressible spheroids with a centrally-concentrated mass. This ratio was at a maximum at an enclosed mass of approximately $100M_{\odot}$. The transition between instabilities identified above is within this radius. This halo fragments into multiple components because of the nesting of this marginal chemical instability within the radius of that of the rotational instability. However, more important is if an increase in this ratio is found exactly at the radii where the cloud has been identified as fragmenting. While analytic estimates for the gravitational potential energy of a cloud vary by factors of order unity depending on the eccentricity and ellipticity of the cloud, the relative ratio traces the mass scales where fragmentation may occur.

The total number of first-generation Population III stars is likely to be significantly smaller than that of the second generation. Assuming no recombination, massive metal-free stars can ionize of order $10^7 M_{\odot}$ of gas, which is between $100 - 1000$ times the gas mass of a Population III star-forming halo (25), and thus will be outnumbered by a large factor by metal-free stars forming in preprocessed regions. Fragmentation in unprocessed, first-generation Population III stars thus indicates that fragmentation in preprocessed, second-generation Population III stars is also possible. This would ultimately be more important to structure formation and the star formation history of the universe and the chemical signature of metal free stellar evolution in the fossil record of old stars in the Galaxy. (26) By changing the size of the gas reservoirs from which the first-generation Population III protostars accrete, as well as the ultraviolet flux from the subsequent metal-free stars themselves, the long-term star formation environment for the next generation of Population III stars could be dramatically changed. A higher flux of ionizing photons could lead to more efficient cooling by molecular hydrogen in neighboring halos (27, 28)

but a lower meta-galactic flux would likely lead to a higher global star formation rate and higher accretion rates. (29)

We have shown that in a particular realization fragmentation occurs at relatively high densities. The separation and timescales are such that the two identified fragments are likely to form a binary stellar system. Improvements to chemical solvers at high densities and better laboratory values for the molecular hydrogen rate coefficients may change the details of the collapse, but these results demonstrate that fragmentation is possible in metal-free halos collapsing from realistic initial conditions. The frequency of such fragmentation, and thus that of metal-free binary systems, cannot be gauged using the small number of simulations conducted thus far.

The problem of “finding” fragmentation in cosmological halos may be one of poor sampling; if fragmentation is rare, the small number of published calculations likely will not sample those halos in which it could occur. In particular, if fragmentation is more likely to occur in halos that undergo rapid merger history, the current means of ab initio simulation of Population III star formation may be ill-equipped to study its likelihood and relevance. We have found fragmentation in one out of five realizations, suggesting that binaries are a formation channel that must be considered in population synthesis studies. From a set of only five realizations an initial mass function cannot be estimated. However, we conclude by noting that the current means of conducting high-dynamic range simulations are biased against finding fragmentation in collapsing pre-stellar clouds. This simulation fragmented at a density of $\simeq 2.0 \times 10^{-13} \text{g cm}^{-3}$, which corresponds to a dynamical time of 210 years; if the time delay between clump formation is greater than approximately the dynamical time, the current methods of simulating primordial star formation will not observe fragmentation. Consequently it is likely that a substantial fraction of Population III stars are forming binaries or event multiple systems.

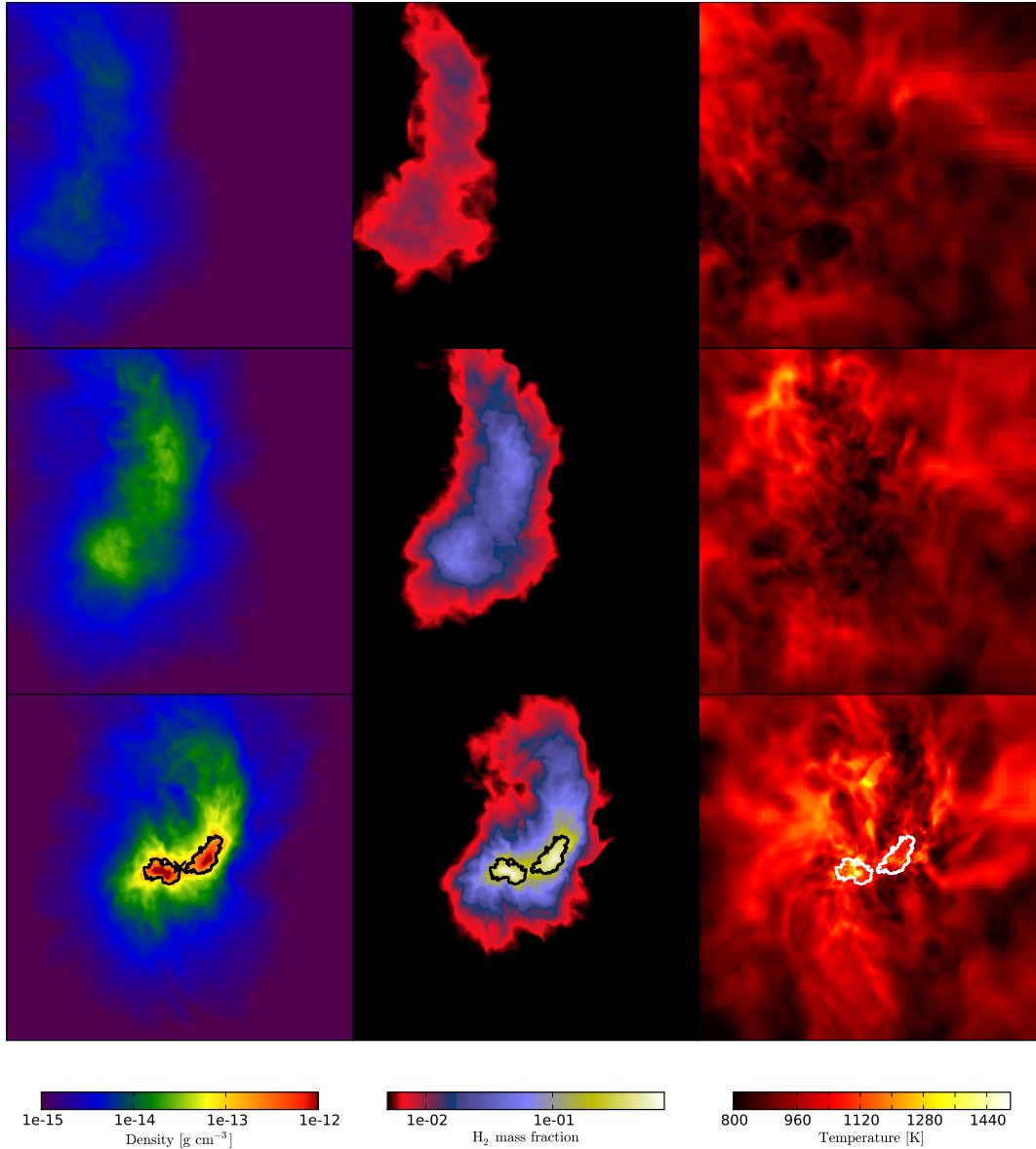


Fig. 1.

Mass-weighted average density (left column), H₂ fraction (middle column), and temperature (right column) projected through a cube centered on the center of mass of the two-core system with a side length of 3500 AU. The bottom row is the final output of the simulation, the middle row is 555 years previous, and the top row is an additional 591 years previous to the middle row (1146 years before the end of the simulation). Gravitationally bound cores with minimum density $3.0 \times 10^{-12} \text{g cm}^{-3}$ have been outlined with thick lines in the bottom row; Core A is on the left and Core B is on the right. Field of view is 3500AU.

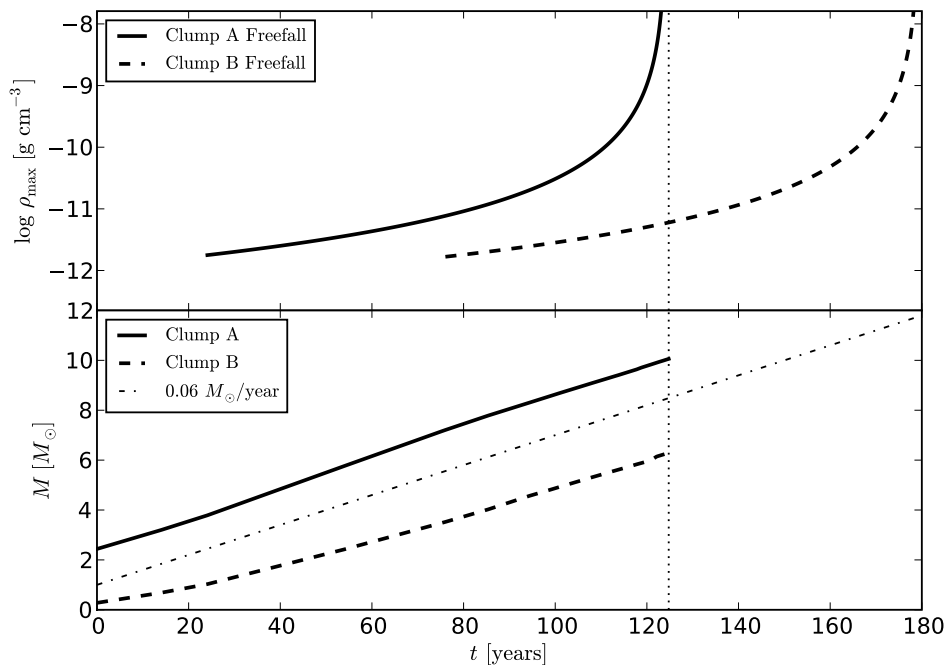


Fig. 2.

Cores, identified by placing a minimum density cut at $3.0 \times 10^{-13} \text{g cm}^{-3}$, plotted over time. The y-position denotes current maximum density, x-position denotes time since the first core was identified. Overlaid is the predicted free-fall evolution of the peak density in each core starting from the first time when the maximum density is greater than $10^{-12} \text{g cm}^{-3}$, governed by $\frac{d\rho}{dt} = -\frac{\rho}{t_{ff}}$, where we use $t_{ff} = \sqrt{\frac{3\pi}{32G\rho_{\max}}}$. We have extended the free-fall trajectories past the end of the simulation, which is indicated by the dotted line.

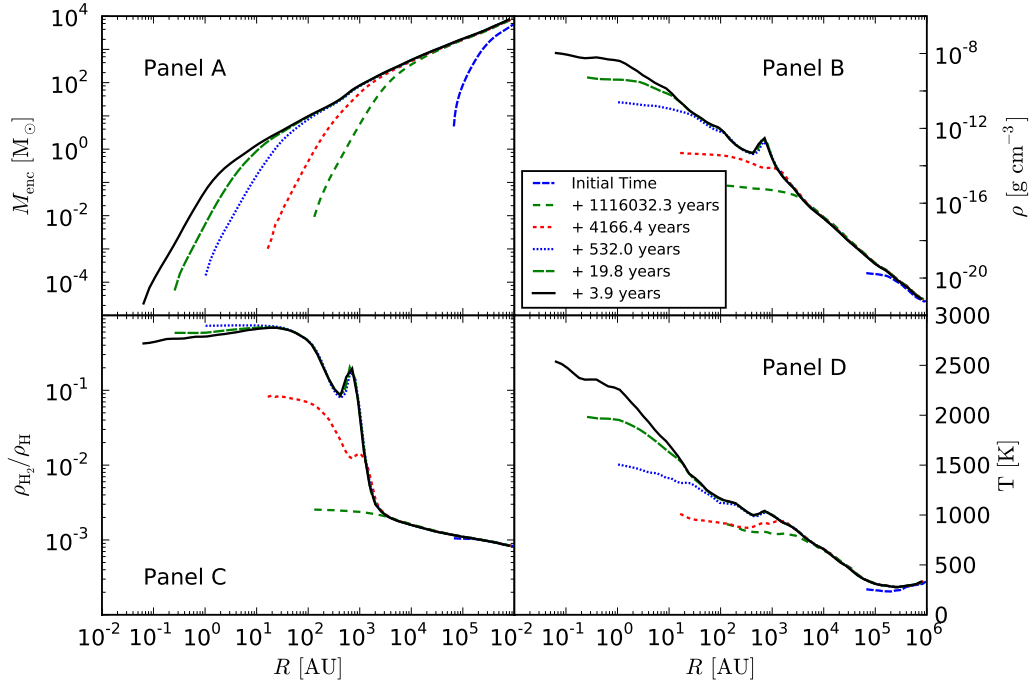


Fig. 3.

Mass-weighted, spherically-averaged quantities as a function of distance from the most dense point (which is located within Core A after the cloud fragments) at different times in the simulation: mass-enclosed as a function of radius (Panel A), density as a function of radius (Panel B), molecular hydrogen mass fraction (Panel C), and temperature (Panel D).

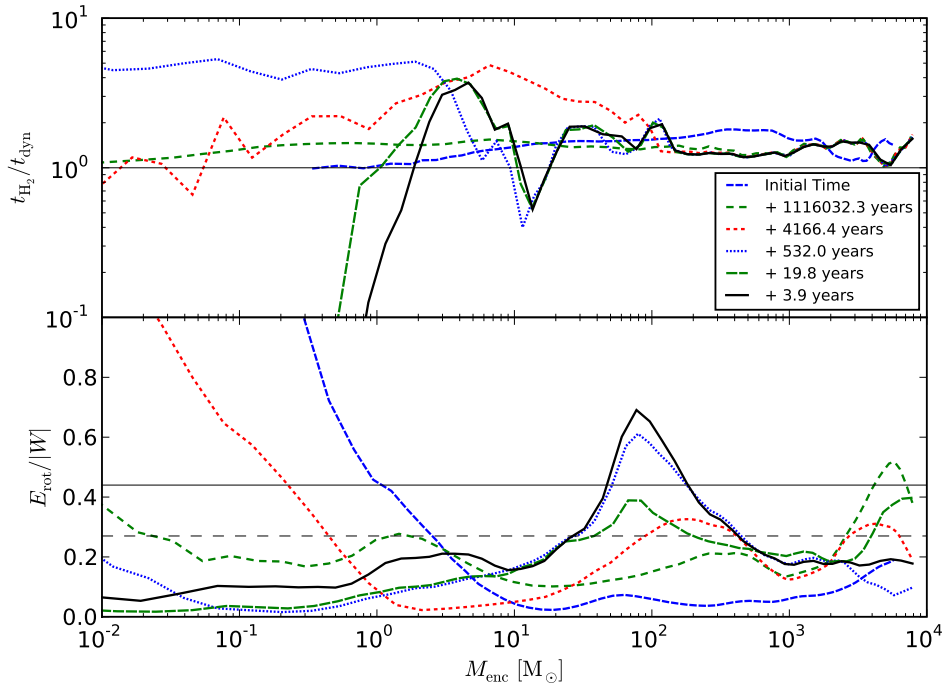


Fig. 4.

Enclosed quantities as a function of mass-enclosed, with respect to the most dense point (which is located within Core A after the cloud fragments) and calculated in the rest frame of that point at different times in the simulation: the mass-weighted average ratio of the dynamical time of the gas divided by the cooling time of the molecular hydrogen, taking into account the heating from three-body formation processes (top panel), and rotational energy divided by gravitational binding energy (bottom panel). In the bottom panel, lines have been drawn to indicate a ratio of 0.27 (thin, dashed) and 0.44 (thin, solid).

Supporting Online Material

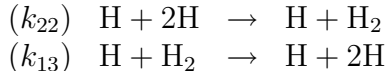
Simulation Methodology

The simulation presented in this work corresponds to simulation L0_30C in (11), which was initialized from Gaussian random initial conditions at redshift $z = 99$ inside a cubic volume with a side length of $300 \text{ kpc } h^{-1}$ (comoving). In addition to standard refinement criteria based on overdensity and cooling time, we require a minimum of 64 cells per Jeans length, ensuring adequate resolution at all stages of collapse, ending with 31 levels of refinement.

The simulations presented here implement a primordial chemistry solver optimized

to be efficient in the stiff regime when three-body reactions forming molecular hydrogen become dominant, utilizing the method from (30). The equation of state of molecular hydrogen is also treated accurately, and all kinetic rate equations are solved without applying prescriptions for equilibria. In contrast to previous adaptive mesh refinement simulations, these calculations include energy contributions due to the formation and destruction of molecular hydrogen as a result of three-body reactions (4.48 eV/molecule), the dominant H₂ formation channel above densities of 10⁻¹⁶g cm⁻³. These energy contributions, as well as energy losses due to radiative processes, are split into formation and destruction contributions and the energy is updated in a second-order backward difference method. This allows for fast numerical convergence during integration. The changes in the gas chemical state are updated on the same timescale as the thermal changes, ensuring accurate chemothermal composition.

For the coefficients governing the formation and dissociation of molecular hydrogen,



we use the rate calculated in (10) where a discussion of the uncertainty governing this particular process is detailed. This uncertainty is further discussed in (31). We have also used a prescription from (9) for the optical depth of ro-vibrational cooling from molecular hydrogen, as well as the optical depth to collision-induced absorption. We have additionally included the formation of molecular hydrogen via three-body reactions with H₂ as the third body, using the rates given in (32). The remaining set of chemical rate coefficients is identical to that of (11).

We have simulated five different cosmological halos, with four of the calculations corresponding to runs from (11). The simulation presented in this work corresponds to simulation L0_30C in (11), which was initialized from Gaussian random initial conditions at redshift $z = 99$ inside a cubic volume with a side length of 300 kpc h⁻¹ (comoving). The other four realizations did not fragment before we stopped each simulation. We initialize the simulation on a 128³ root grid with three nested levels of refinement, for an effective resolution of 1024³ (0.42 kpc proper at $z = 99$). Our finest dark matter particle mass is 2.6M_⊙. The first protostar forms at redshift $z = 19.08$, inside a dark matter halo of mass $5.8 \times 10^5 M_{\odot}$ with a gas spin parameter of 0.025 and dark matter spin parameter of 0.042, where the spin parameter is defined as:

$$\lambda = \frac{L|E|^{1/2}}{GM^{3/2}}$$

where L is the mass-weighted average specific angular momentum, E is the total kinetic energy and M is the enclosed mass. This collapse time is somewhat delayed from that in (11), which we attribute to different choices of molecular hydrogen formation rate and cooling rates; however, the two simulations are in general agreement. The simulation was stopped at a maximum (proper) baryon density of 1.61×10^{-8} g cm⁻³ ($n_{\text{H}} \sim 10^{16}$ cm⁻³),

at a redshift of 19.08, with 31 levels of refinement. The peak spatial resolution is $1.72 R_{\odot}$ (proper) and at the end of the simulation there were $8.75 \times 10^7 \approx 440^3$ unique computational elements with a final mass resolution of $\approx 10^{-7} M_{\odot}$.

Quantities

We tabulate several relevant quantities of the two cores in Table 1. These values have all been calculated during the final output from the simulation, when the maximum baryon density was $1.61 \times 10^{-8} \text{g cm}^{-3}$.

Resolution Studies

We have conducted resolution studies of this particular realization. With the refinement criteria such that we had 16 cells per Jeans length (J16), we allowed the simulation to run until the maximum density was 10^{-5}g cm^{-3} , where we observed that two cores had formed with a separation of ~ 200 AU and masses of two and seven solar masses, with topologically distinct, gravitationally-bound density contours at a density of $9.5 \times 10^{-13} \text{g cm}^{-3}$. The separation was found to be lower than the Keplerian radius. To ensure that this fragmentation was not the result of resolution-limited fragmentation, we restarted the simulation from the time when the maximum density was $10^{-21} \text{g cm}^{-3}$, before the onset of rapid molecular hydrogen formation. With a total of 32 cells per Jeans length (J32), we saw fragmentation at length scales of ~ 100 AU. However, because of the close pair distance, it is unclear whether or not the cores would subsequently merge. The work presented here had the greatest resolution, requiring 64 cells per Jeans length (J64).

By changing the required resolution, we have changed the structure of the hydrodynamic flow into the collapsing region. The delay time in the simulation corresponded roughly to the strength of fragmentation; J32 collapsed the earliest, with J16 collapsing 6000 years later and J64 collapsing 175,000 years following that. This corresponds to roughly 8% of the freefall time at the density at which we restarted the simulation. The actual collapse takes about 5 million years because of the balance of molecular cooling and heat input from turbulence on the large scales ($\sim \text{pc}$) as hitherto seen and explained by (20). As we conduct the resolution study varying the spatial resolution by a factor 4 one also slightly modifies the “initial conditions” since we start the calculation not shortly after recombination, where the original simulation was initialized, but rather at an intermediate time. The loitering phase relevant for primordial star formation otherwise will always be prone to the intermittency issues known so well in interstellar turbulence. Nevertheless, looking at the difference between the J16 and J32 runs the slight change in “initial conditions” only lead to a 6000 year difference. The timing clearly is the most significant differences in these runs.

Core Finding Algorithm

We identified cores by using an optimized version of the core finder described in (33). Starting with a sphere of radius 2500AU in radius, centered at the most dense point in the simulation, we recursively identify topologically connected sets of cells of a given density minimum, incrementing the density minimum with every subset of the data that is extracted. All sets of cells that are not gravitationally bound are eliminated, as are objects with only a single subset identified. This allows us to identify the largest topologically connected sets of cells that are gravitationally bound.

In this algorithm we compute the gravitational energy by direct summation, rather than using the potential Enzo computes. Consequently the computational cost scales with N^2 where N is the number of cells in the simulation. As such, performing this computation on commodity CPUs became cost prohibitive; to that end, we converted the code to run on the NVidia CUDA framework¹. This decreased computational time substantially, allowing us to perform finely-spaced sweeps of density-space (separated by 0.15 dex), ensuring we have accurately identified fragments.

References and Notes

1. T. Abel, G. L. Bryan, M. L. Norman, *Science* **295**, 93 (2002).
2. N. Yoshida, K. Omukai, L. Hernquist, *Science* **321**, 669 (2008).
3. V. Bromm, A. Loeb, *New Astronomy* **9**, 353 (2004).
4. K. Omukai, F. Palla, *ApJ* **589**, 677 (2003).
5. C. F. McKee, J. C. Tan, *ApJ* **681**, 771 (2008).
6. K. Omukai, R. Nishi, *ApJ* **508**, 141 (1998).
7. E. Ripamonti, T. Abel, *MNRAS* **348**, 1019 (2004).
8. J. C. Tan, C. F. McKee, *ApJ* **603**, 383 (2004).
9. E. Ripamonti, T. Abel, *MNRAS* **348**, 1019 (2004).
10. S. Glover, *First Stars III*, B. W. O’Shea, A. Heger, T. Abel, eds. (2008), vol. 990 of *American Institute of Physics Conference Series*, pp. 25–29.
11. B. W. O’Shea, M. L. Norman, *ApJ* **654**, 66 (2007).
12. N. Yoshida, K. Omukai, L. Hernquist, T. Abel, *ApJ* **652**, 6 (2006).

¹<http://www.nvidia.com/cuda/>

13. M. J. Turk, T. Abel, B. W. O'Shea, *First Stars III*, B. W. O'Shea, A. Heger, T. Abel, eds. (2008), vol. 990 of *American Institute of Physics Conference Series*, pp. 16–20.
14. V. Bromm, P. S. Coppi, R. B. Larson, *ApJ* **564**, 23 (2002).
15. F. Nakamura, M. Umemura, *ApJ* **548**, 19 (2001).
16. K. Saigo, T. Matsumoto, M. Umemura, *ApJ* **615**, L65 (2004).
17. P. C. Clark, S. C. O. Glover, R. S. Klessen, *ApJ* **672**, 757 (2008).
18. M. N. Machida, K. Omukai, T. Matsumoto, S.-i. Inutsuka, *ApJ* **677**, 813 (2008).
19. V. Bromm, P. S. Coppi, R. B. Larson, *ApJ* **527**, L5 (1999).
- O'Shea et al.(2004). O'Shea, B. W., Bryan, G., Bordner, J., Norman, M. L., Abel, T., Harkness, R., & Kritsuk, A. 2004, arXiv:astro-ph/0403044
20. N. Yoshida, T. Abel, L. Hernquist, N. Sugiyama, *ApJ* **592**, 645 (2003).
21. E. C. Ostriker, *ApJ* **513**, 252 (1999).
22. K. Omukai, Y. Yoshii, *ApJ* **599**, 746 (2003).
23. I. Hachisu, J. E. Tohline, Y. Eriguchi, *ApJS* **66**, 315 (1988).
24. I. Hachisu, J. E. Tohline, Y. Eriguchi, *ApJ* **323**, 592 (1987).
25. T. Abel, J. H. Wise, G. L. Bryan, *ApJ* **659**, L87 (2007).
26. J. Tumlinson, *ApJ* **641**, 1 (2006).
27. B. W. O'Shea, T. Abel, D. Whalen, M. L. Norman, *ApJ* **628**, L5 (2005).
28. J. H. Wise, T. Abel, *ApJ* **685**, 40 (2008).
29. B. W. O'Shea, M. L. Norman, *ApJ* **673**, 14 (2008).
30. J. G. Verwer, *SIAM J. Sci. Comput* **15**, 1243 (1994).
31. S. C. O. Glover, T. Abel, *MNRAS* **388**, 1627 (2008).
32. F. Palla, E. E. Salpeter, S. W. Stahler, *ApJ* **271**, 632 (1983).
33. B. D. Smith, M. J. Turk, S. Sigurdsson, B. W. O'Shea, M. L. Norman, *ApJ* **691**, 441 (2009).

34. We thank V. Bromm, G. Bryan, A. Escala, S. Glover, C. McKee, J. Oishi, B. Smith, J. Tumlinson, and N. Yoshida for useful discussions. This work was partially supported by the U.S. Department of Energy contract to SLAC no. DE-AC02-76SF00515, NASA ATRP grant NNX08AH26G and NSF AST-0807312. BWO and MJT carried out this work in part under the auspices of the National Nuclear Security Administration of the U.S. Department of Energy at Los Alamos National Laboratory under Contract No. DE-AC52-06NA25396. BWO was partially supported by a LANL Director*s Postdoctoral Fellowship (DOE LDRD grant 20051325PRD4).

Core	ρ_{\max}	Mass	\bar{R}	t_{ff}
A	$1.61 \times 10^{-8} \text{g cm}^{-3}$	$10.0M_{\odot}$	24.4 AU	0.52 years
B	$5.03 \times 10^{-12} \text{g cm}^{-3}$	$6.3M_{\odot}$	98 AU	29.7 years

Table 1: Table of quantities for identified gas cores from final simulation output